Continental Shelf Research 30 (2010) 2027–2042

Contents lists available at ScienceDirect

Continental Shelf Research

journal homepage: www.elsevier.com/locate/csr

Modeling the timing of spring phytoplankton bloom and biological production of the Gulf of St. Lawrence (Canada): Effects of colored dissolved organic matter and temperature

Zhi-Ping Mei [a,*,1], François J. Saucier [a,2], Vincent Le Fouest [b], Bruno Zakardjian [c], Simon Sennville [a], Huixiang Xie [a], Michel Starr [d]

[a] Institut des Science de la Mer de Rimouski (ISMER), Université du Québec à Rimouski, Rimouski, Québec, Canada G5L 3A1
[b] Laboratoire d'Oceanographie de Villefranche, BP 8, CNRS & Univ. Pierre et Marie Curie (Paris VI), 06238 Villefranche-sur-Mer Cedex, France
[c] Université du Sud Toulon-Var, LSEET-LEPI, Bâtiment F, BP 20132, 83957 La Garde Cedex, France
[d] Institut Maurice-Lamontagne, Direction des Sciences Océaniques Ministère des Pêches et Océans CP 1000, Mont-Joli, Québec, Canada G5H 3Z4

ARTICLE INFO

Article history:
Received 14 January 2010
Received in revised form
23 September 2010
Accepted 5 October 2010
Available online 14 October 2010

Keywords:
Gulf of St. Lawrence
Marine ecosystem model
Temperature
CDOM
Phytoplankton bloom
Biological production

ABSTRACT

The effects of colored dissolved organic matter (CDOM) from freshwater runoff and seasonal cycle of temperature on the dynamic of phytoplankton and zooplankton biomass and production in the Gulf of St. Lawrence (GSL) are studied using a 3-D coupled physical-plankton ecosystem model. Three simulations are conducted: (1) the reference simulation based on Le Fouest et al. (2005), in which light attenuation by CDOM is not considered and maximum growth rate (μ_{max}) of phytoplankton and zooplankton are not temperature-dependent (REF simulation); (2) light attenuation by CDOM is added to REF simulation (CDOM simulation); and (3) in addition to CDOM, the μ_{max} of phytoplankton and zooplankton are regulated by temperature (CDOM+TEMP simulation). CDOM simulation shows that CDOM substantially reduces phytoplankton biomass and production in the Lower St. Lawrence Estuary (LSLE), but slightly reduces overall primary production in the GSL. In the LSLE, the spring phytoplankton bloom is delayed from mid-March to mid-April, resulted from light attenuation by CDOM. The CDOM+TEMP simulation shows that the spring phytoplankton bloom in the LSLE is further delayed to July, which is more consistent with observations. Annual primary production is reduced by 33% in CDOM+TEMP simulation from REF and CDOM simulations. Zooplankton production is the same in all three simulations, and export of organic matter to depth is reduced in CDOM+TEMP simulation, suggesting that temperature controlled growth of phytoplankton and zooplankton enhances the coupling between primary production and zooplankton production under the seasonal temperature cycle of the GSL.

1. Introduction

The Gulf of St. Lawrence (GSL) is located in eastern Canada at the lower limit of Subarctic region. It is an important fishing ground of Maritime provinces of Canada, producing about 25% of total commercial fish catch by weight of Canada (Dickie and Trites, 1983; Chadwick and Sinclair, 1991), and the transport corridor between central and eastern Canada and North Atlantic. Biogeochemically, it connects the Great Lakes of North America to the Atlantic Ocean. The GSL receives terrestrial organic matter along with freshwater from Great Lakes upstream, and numerous rivers surrounding the GSL (Koutitonsky and Bugden, 1991) (Fig. 1). The impact of nutrient flux from the GSL reaches the Scotian Shelf (Petrie and Yeats, 2000), and Georges Bank (Houghton and Fairbanks, 2001). Freshwater pulses from the rivers are the main forcing of buoyancy-driven circulation of the GSL and govern the distribution of phytoplankton in the estuary (Savenkoff et al., 1997). Freshwater runoff induces cross-frontal current and upwelling in the Gaspé currents, which contribute to enhanced biological productivity (Bugden et al., 1982). Levasseur et al. (1992) estimated about 85–90% of seaward nutrient flux was from St. Lawrence estuary. That may explain why the crustacean and finfish landing in the Gulf are correlated with freshwater runoff.

The CDOM and other suspended materials carried into the GSL with riverine freshwater discharge have a strong impact on the optical properties of the surface water of the GSL (Nieke et al., 1997; Yeats, 1988), reducing the irradiance available to phytoplankton

* Corresponding author. Tel.: +1 410 221 8288.
E-mail addresses: zmei@mta.ca, zmei@umces.edu (Z.-P. Mei), lefouest@obs-vlfr.fr (V. Le Fouest), Bruno.Zakardjian@lseet.univ-tln.fr (B. Zakardjian), simon_senneville@uqar.qc.ca (S. Sennville), huixiang_xie@uqar.qc.ca (H. Xie), Michel.Starr@dfo-mpo.gc.ca (M. Starr).
[1] Current address: University of Maryland Center for Environmental Science, Horn Point Laboratory, PO Box 775, Cambridge, MD 21613, USA.
[2] Deceased.

0278-4343/$ - see front matter © 2010 Elsevier Ltd. All rights reserved.
doi:10.1016/j.csr.2010.10.003

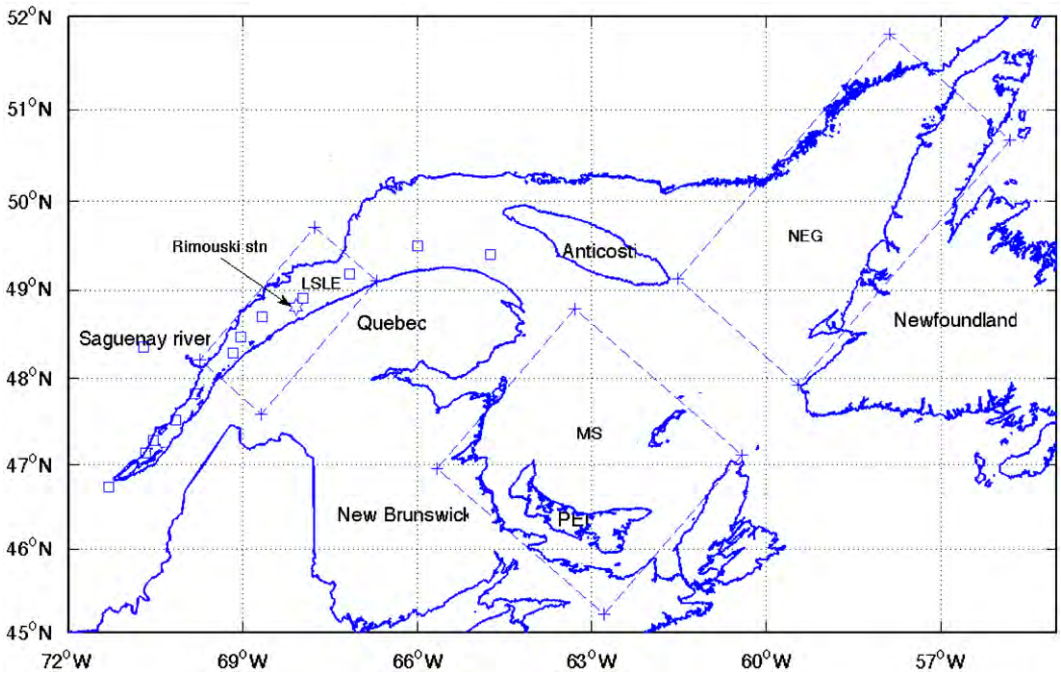

Fig. 1. The map of Gulf of St. Lawrence. Four subregions, lower St. Lawrence estuary (LSLE), Magdalen shallow (MS) and northeast gulf (NEG), are identified for detailed time series analysis of phyto- and zooplankton biomass and production. The time series station of Rimouski Station is located as a star in the LSLE. Squares are locations of the stations sampled for CDOM. Note one station for St. Lawrence River and one station in Saguenay fjord are outside the model domain, but serve to provide CDOM in freshwater flowing to GSL.

photosynthesis and interfering with the retrieval of chlorophyll concentration (Chl) from satellite remote sensing (Branco and Kremer, 2005; Blough and Del Vecchio, 2002; Coble et al., 2003; Nelson and Siegel, 2002; Smyth et al., 2005). CDOM may also be formed through photochemical transformation of dissolved organic matter of terrestrial origin and phytoplankton photosynthesis, and consumed through photobleaching (Kieber et al., 1997; Whitehead et al., 2000).

The timing of spring phytoplankton blooms in the GSL may vary with interannual variability of ocean physics, but usually the spring phytoplankton bloom in the lower St. Lawrence Estuary (LSLE, Fig. 1) is later (June–July) than in the northeast gulf (NEG) and southern gulf (Magdalen shallow, MS) in April–May (de Lafontaine et al., 1991; Therriault and Levasseur, 1985; Levasseur et al., 1984; Roy et al., 2008). The timing of spring phytoplankton bloom has important consequences to the survival of zooplankton and thus fishes larvae and their recruitment in coastal waters. In the southeast of the Scotia Shelf, the timing of the spring phytoplankton bloom explains 89% of the interannual variability in the survival of larval haddock (*Melanogrammus aeglefinus*) (Platt et al., 2003). This is expected to apply to GSL as well, based on Cushing's match and mismatch hypothesis (Cushing, 1990).

There are two hypothesis regarding the later spring phytoplankton bloom in the LSLE than in gulf in the GSL. Firstly, the turbidity mainly due to CDOM from freshwater runoff delayes the spring phytoplankton bloom in the LSLE (de Lafontaine et al., 1991; Therriault and Levasseur, 1985). Observations in April and May, however, suggest that during these months mean irradiance in the mixed layer in the LSLE is sufficient for phytoplankton bloom to start based on Sverdrup's model (Levasseur et al., 1984). An alternative hypothesis is also related to freshwater runoff. Strong current resulted from freshwater runoff during spring peak of ice and snow melt in the catchment area prevents phytoplankton biomass from building up (Zakardjian et al., 2000).

The GSL has a strong seasonal and interannual variability in physics. It is completely ice covered during winter, and open water begins in spring-summer. The water column is strongly mixed in winter, with maximum mixed layer depth of 100 m, and becomes highly stratified in summer. Water temperature at the surface is at freezing point in winter, and reaches as high as $>25\ ^{\circ}$C at surface in summer (Saucier et al., 2003). Interannual variability of climate forcing changes due to freshwater input from rivers, ice cover, water column mixing, and temperature. The large variations of the physics of the GSL will strongly affect the growth of phytoplankton and zooplankton at spatial, seasonal and interannual scales. Levasseur et al. (1984) showed that the phytoplankton biomass in the LSLE is strongly correlated with water temperature. It has been reported that zooplankton biomass is reduced in colder years, and their production increases with boreal-temperate species developed in warmer years in the GSL (de Lafontaine et al., 1991, and references therein). These indicate plankton communities respond sensitively to temperature change in the GSL.

In order to understand the physical mechanisms controlling the dynamic of planktonic ecosystem in the GSL, a 3-D coupled physical-plankton ecosystem model of the GSL was developed by Le Fouest et al. (2005). Seasonal development of primary and secondary production of the GSL was simulated, and heterogenous plankton ecosystem processes were revealed to associate with mesoscale variability of hydrodynamics across the GSL (Le Fouest et al., 2005). The model, however, did not consider the effects of CDOM and temperature dependence of the maximum growth rates ($\mu_{\max}$ d^{-1}) of phytoplankton and zooplankton. In a subsequent study, Le Fouest et al. (2006) implicitly simulated the effect of riverine CDOM, which is diagnosed from salinity based on the linear relationship between light attenuation coefficient and salinity, on primary productivity in the estuarine region of the GSL. However, the variability of salinity and CDOM are driven by different processes. Freshwater discharge, precipitation and melting of sea-ice decrease salinity proportional to their amount as their salinity are close to 0, but CDOM concentrations vary depending on the sources of freshwater and their respective amount, and the season of runoff.

For example, CDOM concentration in the Saguenay River on the north shore of the LSLE is much higher than other rivers, even though their salinity is the same (Xie, unpublished). Therefore, it is necessary to simulate CDOM explicitly as a passive tracer in the coupled model.

Temperature–μ_{max} relationship of phytoplankton has been established since Eppley (1972). Recently, Rose and Caron (2007) confirm the temperature–μ_{max} relationship of phytoplankton, by including new data after Eppley (1972), and further establish temperature–μ_{max} relationships for bacteria and zooplankton at different trophic levels. They find the slopes for the temperature–μ_{max} relationships are significantly different between phytoplankton and zooplankton. The μ_{max} of autotrophic plankton is higher than that of zooplankton at lower temperature ranges, but closer to or lower than zooplankton at higher temperature ranges. That affects the timing and extent of phytoplankton bloom in spring–summer in the oceans of different latitudes. Such temperature-based parameterization of μ_{max} of plankton is considered robust and mechanistically based (Caron and Rose, 2008; López-Urrutia, 2008), and when used, may reduce the number of free parameters of plankton ecosystem model. However, differential temperature dependence of phytoplankton and zooplankton growths has rarely been taken into account in marine ecosystem models (Tian, 2006). Inter-model comparisons show that divergence of model performance is strongly linked to how the effects of temperature on phytoplankton production is formulated (Carr et al., 2006).

The objectives of the present study are to understand the importance of CDOM and temperature in affecting the timing of spring phytoplankton bloom in different regions of the GSL, and biological productivity of the entire GSL. In order to test the above hypothesis regarding the timing of spring phytoplankton bloom, we simulate the CDOM dynamically in the coupled physical-plankton ecosystem model of Le Fouest et al. (2005) and to include light attenuation by CDOM. Furthermore, the μ_{max} of phytoplankton and zooplankton is defined as temperature-dependent parameter based on Rose and Caron (2007). The interannual variability of CDOM and temperature will have consequences to that of biological productivity of the GSL.

2. Model

The goal of this study is to understand how CDOM and temperature affect the timing of spring phytoplankton bloom and biological production. We compare the seasonal cycles of phytoplankton and zooplankton biomass and production simulated with the 3-D coupled physical–biological model developed for the GSL (Le Fouest et al., 2005), after the model is modified to account for CDOM in regulating water column irradiance and temperature in regulating μ_{max} of phytoplankton and zooplankton. Particularly, we want to understand why the spring phytoplankton bloom is later in the LSLE than in the Gulf. Therefore, we compare the seasonal cycles of phytoplankton and zooplankton biomass and production of different regions, including the LSLE, NEG and MS in the three simulations as detailed below. Those subregions are defined based on topography and biological dynamics of the GSL (Steven, 1971; de Lafontaine et al., 1991). The LSLE is characterized with low salinity, cold, and high nutrients from rivers and upwelling at the head of Laurentian Channel. The NEG is northern half of the gulf, north of the Laurentian Channel. It is relatively deep (>200 m), and receives Labrador water through Strait of Belle-Isle, with salinity >30. The MS is the southern half of the gulf, and is shallow (average depth of 50 m) and warmer than the LSLE and NEG.

Three numerical experiments are conducted as shown in Table 1. Basic model parameters for the reference simulation (REF simulation) are listed in Table 2, and are the same as Le Fouest et al. (2005). In the REF simulation, light attenuation is contributed from Chl, (k_{Chl}), water (k_w) and non-Chl material (k_p) (Table 2). k_p was tuned to obtain the euphotic zone depths of about 40–50 m observed in the oceanic Gulf water by Doyon et al. (2000) (Le Fouest et al., 2005), and thus represents attenuation of light by CDOM and other detritus in the oceanic Gulf water, but much too low for the LSLE, where light attenuation by CDOM is much stronger and the euphotic zone depths range from 10 to 20 m (Nieke et al., 1997). The CDOM simulation is a modification of the REF simulation in which k_p of the REF simulation is replaced with light absorption by CDOM, the latter is explicitly simulated as a passive tracer. It is assumed here that the attenuation of non-Chl a material are dominantly due to CDOM. k_p in the REF simulation is quite close to the attenuation by CDOM simulated for the oceanic Northeast Gulf (Fig. 4), suggesting CDOM dominates the attenuation of non-Chl a material in oceanic water of the GSL. In the LSLE, the highest attenuation due to CDOM reaches 0.30 m^{-1}, which agrees with the maximum attenuation coefficient in the dataset of Le Fouest et al. (2006). The intercept (0.98) for the relationship between salinity (>27) and light absorption by CDOM (A_{CDOM}) (Eq. (3)) is close to that for the relationship between salinity (>24) and k_p of Le Fouest et al. (2006). Therefore, it is justified to replace k_p of REF simulation with light absorption by CDOM to represent non-Chl light attenuation for the GSL. With CDOM being simulated as a passive tracer, CDOM simulation can resolve spatial, and temporal dynamic of non-Chl light attenuation associated with freshwater runoff. In the future light attenuation by other particles, such as suspended sediments need to be quantified. However, suspended sediment might have settled in the upstream of the estuary, since Nieke et al. (1997) find that the euphotic zone depths in the LSLE are mainly determined by phytoplankton biomass and CDOM. The CDOM+TEMP simulation is a modification of the CDOM simulation, where μ_{max} of phytoplankton and zooplankton are temperature dependent (see details in Section 2.3).

Table 1
The design of numerical experiments.

Simulations	μ_{max} (d^{-1})	Light attenuation components
REF	Constant	Water+Chl+k_p[a]
CDOM	Constant	Water+Chl+CDOM
CDOM+TEMP	$\mu_{max}=f(T)$[b]	Water+Chl+CDOM

[a] Attenuation due to detrital materials, set as a constant (Table 2).
[b] See Eqs. (5)–(7) (Rose and Caron, 2007).

2.1. Coupled physics-biological model

A simple biological model composed of nutrients, phytoplankton, zooplankton and detritus (NPZD) is coupled to the 3-D regional ice-ocean circulation model developed for the GSL (Saucier et al., 2003) as in Le Fouest et al. (2005). The ice-ocean circulation model of Saucier et al. (2003) is forced with air temperature, wind intensity, dew point, cloud cover, precipitation minus evaporation, daily river runoff and area-averaged accumulated and compacted snow depth over the ice. Those atmospheric and hydrologic forcing, plus radiation that forces ecosystem model, are the output of regional and global multiscale climate models (Saucier et al., 2003).

There are a few modifications to the NPZD model of Le Fouest et al. (2005). In Le Fouest et al. (2005), surface irradiance of each grid was discounted by the fraction of a model grid covered with ice, and the irradiance corrected for ice cover was used to calculate light limitation to phytoplankton growth of each grid. In the present study, phytoplankton growth for ice covered and ice free parts of a grid are calculated separately, and then weighted mean growth rate of ice-covered and ice-free areas of each grid is calculated. This is to take into

Table 2
List of symbols and model parameters for reference simulation.

Symbol	Variable name	Parameter values	Reference
Light			
k_w	Attenuation of water	0.04 m^{-1}	Morel (1988)
k_p	Attenuation by non-Chl a materials	0.04 m^{-1}	Fitted
Phytoplankton			
$k3_{LP}$	Half-saturation constant for NO_3 uptake of LP	1 mmol N m^{-3}	Parsons et al. (1984)
$k4_{LP}$	Half-saturation constant for NH_4 uptake of LP	0.5 mmol N m^{-3}	
$k3_{SP}$	Half-saturation constant for NO_3 uptake of SP	1 mmol N m^{-3}	
$k4_{SP}$	Half-saturation constant for NH_4 uptake of SP	0.1 mmol N m^{-3}	
ke	Half-saturation constant for photosynthesis	10 Einst m^{-2} d^{-1}	Kiefer and Mitchell (1983)
dt_{min}	Minimum doubling time of LP and SP	0.5 day	Zakardjian et al. (2000)
$m_{LP,\ SP}$	Senescence of LP and SP	0.02 d^{-1}	Fitted
sed_{LP}	Sinking speed of LP	1 m d^{-1}	Smayda (1970)
C:Chl	Carbon to Chl ratio	55 gC g Chl^{-1}	
Zooplankton			
g^{MEZ}_{max}	MEZ maximum grazing rate	0.2 d^{-1}	Fitted
g^{MIZ}_{max}	MIZ maximum grazing rate	2 d^{-1}	Strom et al. (2001)
iv_{MEZ}	Ivlev parameter of MEZ grazing formulation	0.8 (mmol N m^{-3})$^{-1}$	Frost (1972)
k_{MIZ}	Half-saturation constant for MIZ grazing	0.8 mmol N m^{-3}	Fitted
ass_{MEZ}	Assimilation efficiency of MEZ	70%	Kiorbøe et al. (1985)
ass_{MIZ}	MIZ growth efficiency	30%	Riegman et al. (1993)
m_{MEZ}	MEZ mortality	0.05 (mmol N m^{-3} d^{-1})$^{-1}$	Fitted
m_{MIZ}	MIZ senescence	0.02 d^{-1}	Fitted
eg	DON egestion by MIZ	30%	Lehrter et al. (1999)
ex	NH_4 excretion by MEZ	0.05 d^{-1}	Saíz and Alcaraz (1992)
Detritus			
sed_{POM}	PON sinking speed	100 m d^{-1}	Turner (2002)
fg	PON fragmentation rate	0.05 d^{-1}	Fasham et al. (1990)
rem	DON remineralization rate	0.4 d^{-1}	Pickard et al. (2000)

account the fact that phytoplankton photosynthesis responds to irradiance level nonlinearly. In the present study, monthly climatology of nitrate (NO_3) profiles in the Strait of Belle-Isle and Cabot Strait is used as boundary conditions of the NPZD model as in Le Fouest et al. (2006).

The detailed equations for the plankton ecosystem model can be found in Le Fouest et al. (2005). Briefly, there are two size-classes of phytoplankton, small non-diatoms, and large diatoms, two size-classes of zooplankton, microzooplankton and mesozooplankton, two nutrient sources, NO_3 and ammonium (NH_4), and two detrital nitrogen, dissolved detritus (DON) and particulate detritus (PON). Phytoplankton production and zooplankton grazing, and decomposition of PON produce DON. PON is from non-grazing death of phytoplankton and zooplankton defecation. The planktonic ecosystem model is a nitrogen-based NPZD model. The specific growth rate of phytoplankton (μ, d^{-1}) is taken as the minimum of light limited growth or nutrient-limited growth, following Liebig's law of minimum:

$$\mu = \mu_{max} \min\left(\frac{PAR}{PAR+ke}, \frac{N}{N+k_N}\right) \quad (1)$$

where *ke* is the half-saturation constant for photosynthesis, k_N, the half saturation constant of NO_3 or NH_4 uptake of large or small phytoplankton, and N is either NO_3 or NH_4. Primary production reported here is total primary production, including NO_3 based new production and NH_4 based regenerated production, and is calculated as the product of phytoplankton biomass (N_P) and μ, or $PP = \mu N_P$, assuming Redfield C:N ratio and constant carbon to Chl ratio (C:Chl) (Table 2). Zooplankton production, including microzooplankton and mesozooplankton, is calculated as the product of their grazing rates and assimilation efficiencies.

2.2. Simulation of colored dissolved organic matter (CDOM)

Le Fouest et al. (2006) diagnoses the light attenuation due to non-chlorophyll detritus (mainly CDOM) from salinity as: $k_p = 0.0364\ S + 1.1942$, and k_p is bounded between 0.26 m^{-1} at salinity of 26 and 0.03 m^{-1} at salinity of 32. Previous study (Nieke et al., 1997) suggests that light absorption due to CDOM further increases with decreasing salinity at salinity range <26. In addition, variability of salinity is not only caused by freshwater runoff from rivers, but also by melting of sea-ice in spring, precipitation and evaporation, which may not change salinity and CDOM in the same proportion. Therefore, in this study, we initialize CDOM based on the linear relationships between salinity and CDOM for two salinity ranges (<27 and >27), and prescribe CDOM to the freshwater at the river mouth. As the freshwater and CDOM enter GSL, CDOM is advected and mixed as other tracers.

The concentration of CDOM is represented by its mean light absorption over the PAR wavelength range (A_{CDOM}, m^{-1}), since the ecosystem model uses bulk PAR without resolving spectral light absorption. The A_{CDOM} is initialized from salinity, based on the linear relationship between salinity and CDOM as shown in the data collected in winter 2005 (Xie, unpublished data). CDOM and salinity were sampled across the estuary and extended to the Gaspé coast (see Fig. 1), covering salinity range between 0 and 32. The relationship between A_{CDOM} and salinity (S) can be described as Eqs. (2) and (3), for salinity <27, and ≥ 27, respectively:

$$A_{CDOM} = -0.01392S + 0.5325 \ (r^2 = 0.9162, n = 6, S < 27) \quad (2)$$

or,

$$A_{CDOM} = -0.02995S + 0.9823 \ (r^2 = 0.9857, n = 6, S > 27) \quad (3)$$

The obtained relationships between A_{CDOM} and salinity of different salinity ranges are consistent with earlier results of Nieke et al. (1997). The strong correlations between salinity and A_{CDOM} suggest that salinity can be reliably used to predict the A_{CDOM} in freshwater and to initialize A_{CDOM} across the GSL. The A_{CDOM} of river water is set to be 0.53 m^{-1}, derived from the intercept of Eq. (2), corresponding to the A_{CDOM} at S of 0. A_{CDOM} from the Saguenay fjord (1.97 m^{-1})

is exceptionally high, and remarkably deviated from the linear relationship described in Eqs. (2) and (3), thus the value of 1.97 m^{-1} was assigned to this particular river. The high A_{CDOM} in Saguenay river is caused by high DOM concentrations and higher percentage of humic substances in DOM than in LSLE (Tremblay and Gagné, 2009).

CDOM enters the GSL via river runoff, and is then transported with currents, as shown in the general equation of tracer advection and diffusion:

$$\frac{\delta C}{\delta t}+u\frac{\delta C}{\delta x}+v\frac{\delta C}{\delta y}+w\frac{\delta C}{\delta z} = \frac{\delta}{\delta x}\left(K_x\frac{\delta C}{\delta x}\right)+\frac{\delta}{\delta y}\left(K_y\frac{\delta C}{\delta y}\right)+\frac{\delta}{\delta z}\left(K_z\frac{\delta C}{\delta Z}\right)+source-sink \quad (4)$$

where C represents passive tracers, such as A_{CDOM}.

The strong linear relationships between A_{CDOM} and S (Eqs. (2) and (3)) in both winter and summer suggest that A_{CDOM} in the GSL is mainly determined by mixing of one endmember with low S but high CDOM, with another with high S but low CDOM. Different slopes of the relationship for low salinity (estuarine), and high salinity (Gulf) waters suggest different hydrodynamic processes in the mixing of two endmembers in two regions (Nieke et al., 1997). Therefore, *source* (e.g. biological production) and *sink* (e.g. photochemical degradation and microbial remineralization) terms in Eq. (4) for A_{CDOM} are set to be 0 in the simulations.

2.3. Temperature regulation of maximum growth rate (μ_{max}) of plankton

In REF and CDOM simulations, the μ_{max} of phytoplankton and zooplankton are set to be constant parameters (Table 2) based on data obtained during phytoplankton bloom (Tamigneaux et al., 1997). That may overestimate the μ_{max} before phytoplankton bloom, and underestimate the μ_{max} when temperature increases. Considering the large spatial and seasonal temperature range in the GSL, the temperature-dependent μ_{max} of phytoplankton and zooplankton are taken into account in the CDOM+TEMP simulation. In the CDOM+TEMP simulation, the relationship between temperature (T) and the maximum growth rate of small and large phytoplankton ($\mu_{max}^{LP,SP}$, d^{-1}), microzooplankton (μ_{max}^{MIZ}), and mesozooplankton (μ_{max}^{MEZ}) are defined according to Rose and Caron (2007), and are listed as Eqs. (5)–(7), respectively:

$$\ln \mu_{max}^{LP,SP} = 0.06T-0.5 \quad (5)$$

$$\ln \mu_{max}^{MIZ} = 0.10T-1.0 \quad (6)$$

$$\ln \mu_{max}^{MEZ} = 0.13T-3.0 \quad (7)$$

The slope for phytoplankton growth (Eq. (5)) is similar to Eppley (1972), but the slopes for zooplankton are higher than that of phytoplankton. Consequently, under low temperature ($<15\ ^{\circ}C$), phytoplankton have growth advantage over zooplankton (Rose and Caron, 2007). The maximum grazing rate of micro- and mesozooplankton (g_{max}^{MIZ} and g_{max}^{MEZ}, respectively) are calculated from μ_{max}^{MIZ} and μ_{max}^{MEZ} (Eqs. (6) and (7)) assuming growth yield of 33% for most of the zooplankton groups at their maximum growth rate (Hansen et al., 1997). This value represents an average growth yield for zooplankton across a variety of taxa groups. Even though most values center around 33%, extreme values range from 10% to 45% (Hansen et al., 1997, Table 7). That may lead to the maximum grazing rate to change accordingly.

2.4. Model-data comparisons

The modeled Chl concentrations are compared with Chl sampled in spring-summer (June) and fall (November). The locations of sample stations can be found in Le Fouest et al. (2005, Fig. 5a). We only compare data within the upper 50 m of the water column. There are total of 375 and 430 discrete data points for June and November, respectively. For Chl determination, discrete samples are filtered into glass fibre filter (GF/F). Chl retained on GF/F filters is extracted with 90% acetone overnight in cool temperature, before fluorometer reading, following the protocol of Mitchell et al. (2002).

Both model output and field data are log transformed, so that they conform with normal distribution. Correlation coefficient (R), standard deviation, root mean square difference ($RMSD$), and normalized bias (B^*) are calculated to validate the model output. R, $RMSD$ and B^* (Friedrichs et al., 2009) are calculated as

$$R=\frac{\sum_{i=1}^{n}(\log C_{o,i}-\overline{\log C_o})(\log C_{m,i}-\overline{\log C_m})}{\sqrt{\sum_{i=1}^{n}(\log C_{o,i}-\overline{\log C_o})^2\sum_{i=1}^{n}(\log C_{o,i}-\overline{\log C_m})^2}} \quad (8)$$

$$RMSD=\sqrt{\frac{1}{N}\sum_{i=1}^{N}(\log C_{m,i}-\log C_{o,i})^2} \quad (9)$$

and

$$B^*=\frac{\overline{\log C_m}-\overline{\log C_o}}{\sigma_o} \quad (10)$$

$C_{m,i}$ and $C_{o,i}$ are modeled and observed Chl values, respectively. σ_o is the standard deviation of observed data, and overbar is mean value.

3. Results

3.1. Model data comparison

The model output of Chl in June and November are compared with Chl data collected in June (Fig. 2a–c) and November (Fig. 2d–f) of 1997, respectively. June and November are the seasons of spring and fall blooms, respectively. In REF and CDOM simulations, the data points of observed vs simulated Chl fall above the 1:1 diagonal line in the range between 0.1 and 1 mg m^{-3}, indicating that the REF and CDOM simulations overestimate phytoplankton biomass in both June and November. The data points of CDOM+TEMP simulations fall on the 1:1 diagonal line better than REF and CDOM simulations, particularly for Chl between 0.1 and 1 mg Chl m^{-3} in June, indicating that simulation of the timing of spring phytoplankton bloom is improved in CDOM+TEMP simulation (Fig. 7).

The statistics, including R, σ and $RMSD$ between the modeled and observed Chl are summarized on Taylor diagrams (Taylor, 2001) (Fig. 3).

Corresponding to the scatterplot in Fig. 2, R is higher for the CDOM+TEMP than REF and CDOM simulations in June, the spring bloom season. However, $RMSD$ and σ for CDOM+TEMP simulation are higher than REF and CDOM simulations in June. In November, the statistics of the three simulations are quite close to each other. We further calculated the standardized bias following Friedrichs et al. (2009) (Table 3). The standardized bias is the lowest in CDOM+TEMP simulation in both June and November.

3.2. Spatial distributions in water temperature and CDOM

Water temperature is close to freezing point in most of the area of the GSL in winter (January–March), and slightly increases to

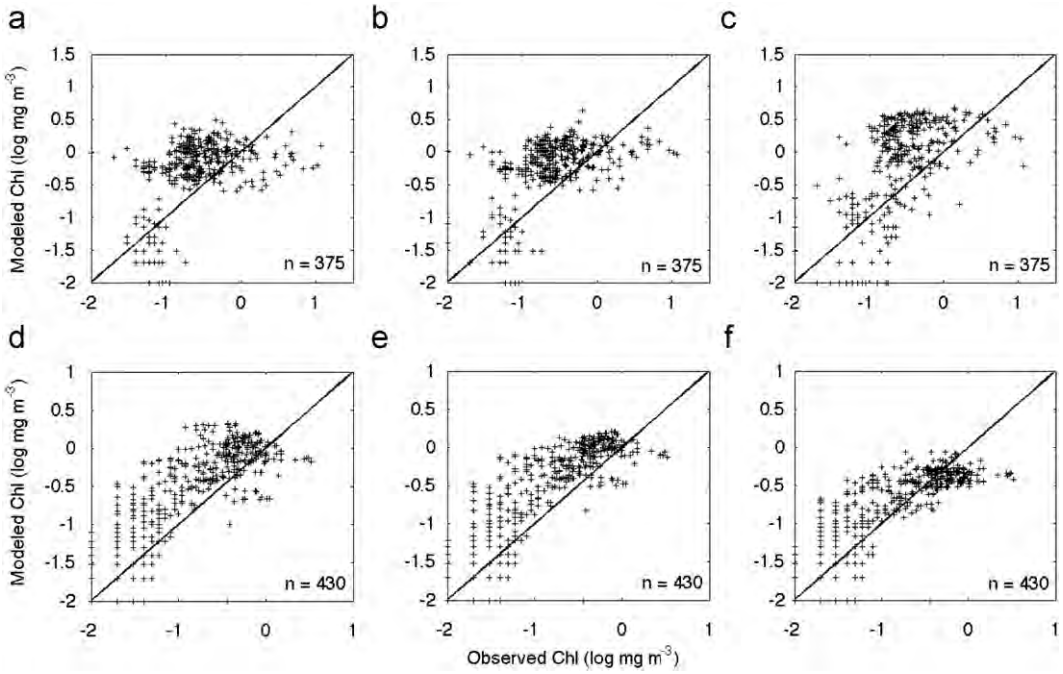

Fig. 2. Scatterplots of modeled (y-axis) vs observed (x-axis) Chl (log mg m^{-3}) for REF (a, d), CDOM (b, e), and CDOM+TEMP simulations (c, f). The dashed line on each panel is 1:1 line. For each simulation, the upper panels are for June (a, b and c), and lower panels (d, e, and f), for November.

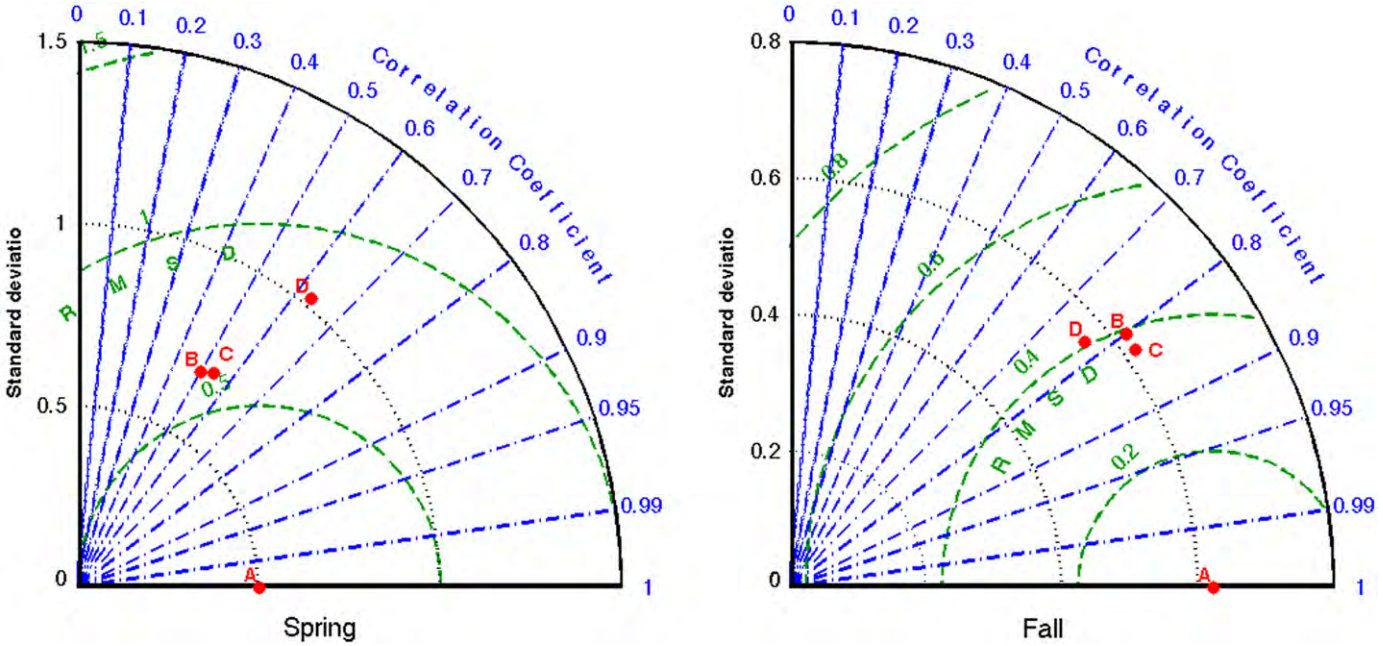

Fig. 3. Taylor diagrams comparing the statistics of simulations against observation data. On each diagram, dash-dot lines indicate correlation coefficient between model and observation, curved broken lines indicate the centered root mean square difference (RMSD) between model and observation data, dotted lines indicate standard deviation of a simulated variable. A is the observation; B, C, and D are REF, CDOM, and CDOM+TEMP simulations, respectively.

around 5–8 °C in the upper estuary, and southeastern coast in spring/summer (April–June). The highest temperature of 20 °C is seen in the southeast of the Gulf, and ~10 °C in the Northeast Gulf (NEG) in summer/fall (July–September), and decreases toward the end of the year. In summer/fall, and fall/winter (October–December), strong temperature gradients can be seen throughout the GSL, with temperature in the southeast being higher than in the northeast and lowest in the LSLE (Fig. 4).

During winter, CDOM distribution is largely limited to the LSLE. In spring/summer, CDOM dramatically increases in the LSLE, the Gaspé current along the coast of the Gaspé peninsula. In summer/fall, CDOM is extended to the downstream of the Gaspé current in the MS. Along with decreasing temperature, CDOM decreases in fall/winter (Fig. 4). The seasonal changes in CDOM is associated with freshwater discharge to the GSL from snow melt on the land and runoff from the surrounding rivers (Nieke et al., 1997).

3.3. Seasonal dynamics of CDOM and temperature in different regions

Detailed physical dynamics of the GSL have been extensively described in Saucier et al. (2003), who showed consistency between modeled and observed fields of salinity and temperature. Here we show mean seasonal dynamics of CDOM and temperature in three subregions, the LSLE, MS, and NEG as shown in Fig. 1.

The LSLE is characterized with the highest CDOM and lowest temperature. The highest CDOM is in mid-April to mid-July, when freshwater runoff is the highest. Temperature in the LSLE is the lowest in the GSL, with the highest temperature of 12 °C at surface water in summer (Fig. 5). The NEG has lowest CDOM, however, is warmer than LSLE, but colder than MS in summer, as NEG is frequently affected by upwelling of cold intermediate water to the surface (Saucier et al., 2003, and references therein). CDOM in the MS is lower than the LSLE, as high CDOM water from the LSLE mixes with low CDOM oceanic water in the gulf via Gaspé current along the Gaspé coast. Seasonal maximum CDOM is between July and September in MS, three months later than in the LSLE. The delay in peak CDOM in MS from the peak of freshwater runoff is attributed to the time required for the surface LSLE water to flow to MS via the Gaspé current. Temperature in the MS is the highest in the GSL due to its lower latitude.

Table 3
Standardized bias for REF, CDOM and CDOM+TEMP simulations against observation in June and November, following Eq. (6) of Friedrichs et al. (2009).

Model	REF	CDOM	CDOM+TEMP
June	0.5116	0.5234	0.3981
November	0.4867	0.5063	0.1193

3.4. Effects of CDOM, and temperature on seasonal dynamics of NO_3, and plankton biomass in different regions

Seasonal dynamics of phytoplankton biomass and NO_3 obtained from three different simulations differ remarkably in the LSLE

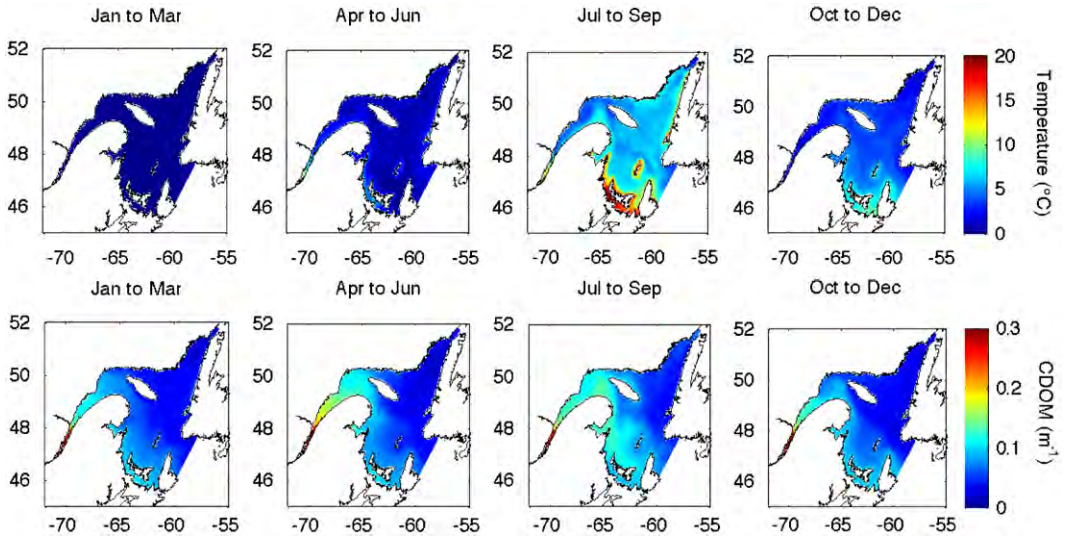

Fig. 4. Seasonal mean water temperature (top 50 m) and CDOM (top 10 m) for winter (January–March), spring/summer (April to June), summer/fall (July–September) and fall/winter (October–December) of the Gulf of St. Lawrence.

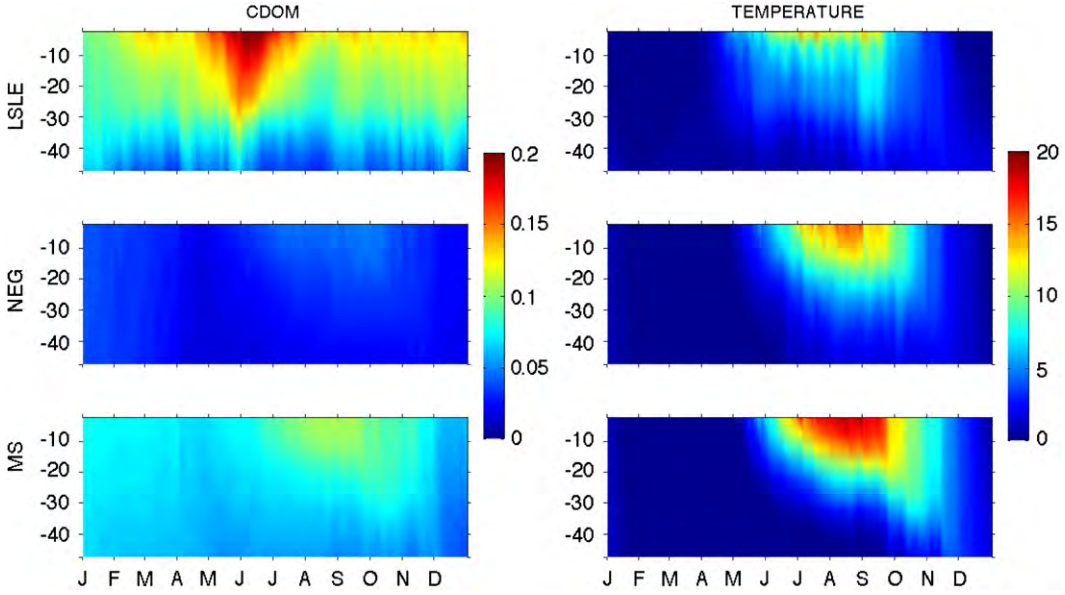

Fig. 5. Seasonal dynamics of CDOM absorption (m^{-1}) and temperature (°C) in three subregions (LSLE, NEG, and MS) of the Gulf of St. Lawrence.

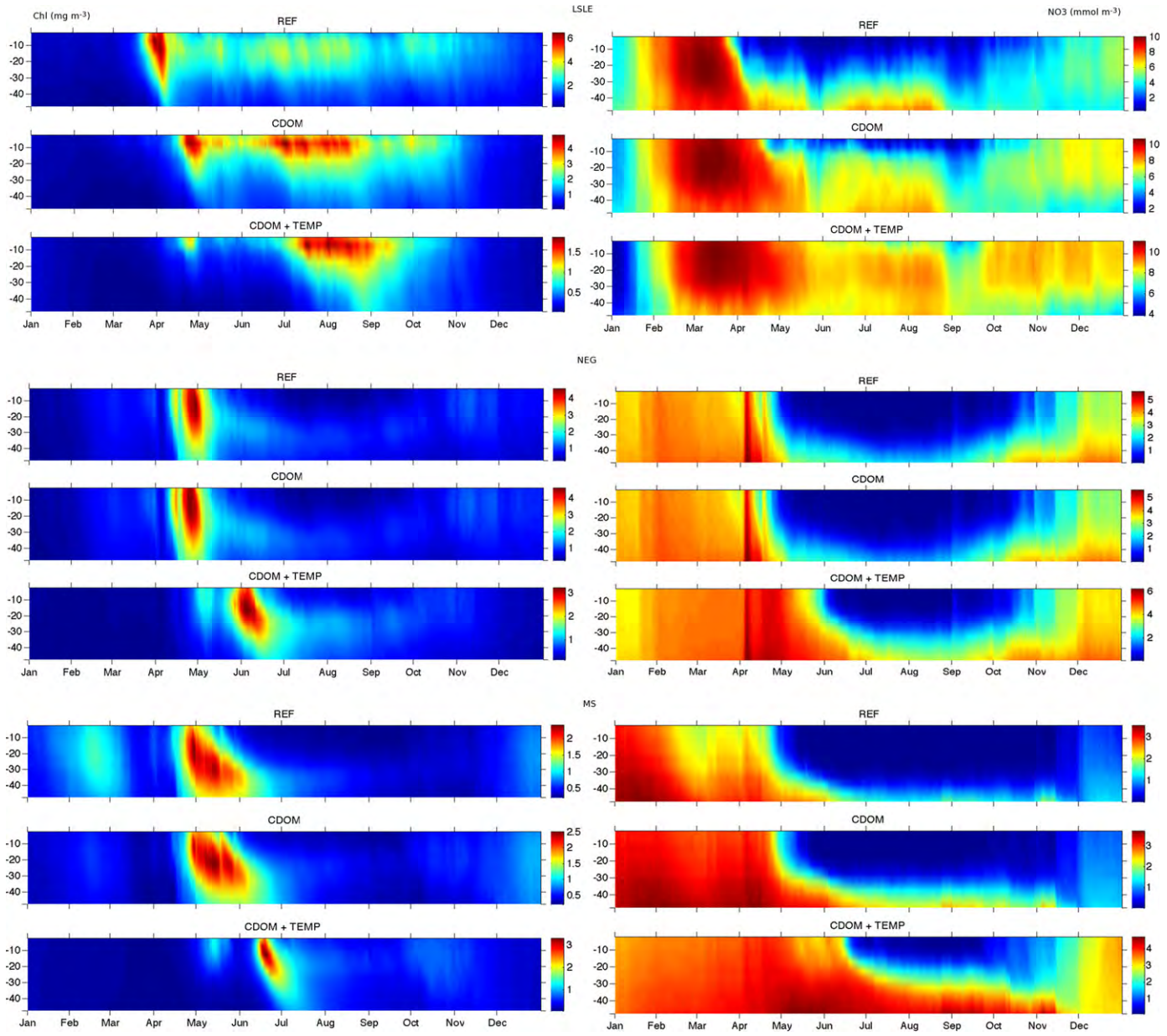

Fig. 6. Time series of Chl (mg Chl m^{-3}) (left) and NO_3 profiles (right) integrated over each of the three sub-regions: LSLE (top), NEG (middle) and MS (lower) for reference simulation (REF), CDOM simulation (CDOM), and temperature dependent plankton growth simulation (CDOM+TEMP).

(Fig. 6). Phytoplankton bloom is delayed to mid-April in CDOM simulation comparing with late March in REF simulation. In CDOM+TEMP simulation, phytoplankton bloom is delayed to July, and the peak phytoplankton biomass is decreased to <2 mg Chl m^{-3}. NO_3 decreases with increased Chl biomass. The depth of nutricline decreased in CDOM simulation from REF simulation, as CDOM decreased the penetration depth of irradiance. The depth of nutricline is as shallow as 10 m in the CDOM+TEMP simulation due to further temperature limitation of phytoplankton growth in lower water column.

Seasonal dynamics of phytoplankton biomass and NO_3 in the CDOM simulation is not different from REF simulation in NEG. In CDOM+TEMP simulation, spring phytoplankton bloom delayed to mid-May and June from mid-April in REF and CDOM simulation. The depths of subsurface Chl maxima and nutricline in CDOM+TEMP are shallower than in REF and CDOM simulations (Fig. 6), indicating lower temperature reduces phytoplankton biomass and NO_3 consumption in the subsurface of the water column.

There is no difference in the timing of spring phytoplankton bloom between REF and CDOM simulations in MS. Spring phytoplankton bloom in CDOM+TEMP simulation is delayed to June. The depths of nutricline and subsurface Chl maxima is shallower in CDOM+TEMP simulation than in REF and CDOM simulation. This shallower nutricline allows nutrient to be upwelled to surface and the fall bloom to develop in October in CDOM+TEMP simulation (Fig. 6). Low NO_3 after spring phytoplankton bloom in NEG and MS is due to stratification which prevented NO_3 in subsurface layer from being mixed to surface until October. Since we do not consider nutrient input from freshwater, seasonal NO_3 cycle is not affected by freshwater input.

We do not have time series Chl data for all the regions of GSL for 1997. The available time series of Chl, plotted in Fig. 7, was collected at

an estuary station (Station Rimouski, see Fig. 1) during April–October of 1997. The major phytoplankton bloom in LSLE started in June–July in 1997. The timing of major phytoplankton bloom in the LSLE of the CDOM+TEMP simulation is more consistent with those of observations (Levasseur et al., 1984; Starr et al., 2004; Roy et al., 2008).

In the LSLE, zooplankton biomass decreased remarkably in CDOM simulation from REF simulation before July. In CDOM+TEMP simulation, zooplankton biomass further reduced from CDOM simulation by about 50% (Fig. 8 top). In the NEG, the peak zooplankton biomass and their timing are quite similar in REF and CDOM simulations. The peak zooplankton biomass in CDOM+TEMP simulation occurs slightly later, but is slightly higher than in REF and CDOM simulations (Fig. 8 middle). In MS, the differences in zooplankton biomass between REF and CDOM simulations are small. Zooplankton biomass in CDOM+TEMP simulation is higher than in REF and CDOM simulations, but the growth season is about 2 weeks shorter than in CDOM simulation.

3.5. *Effects of CDOM and temperature on primary and secondary production, and export of organic matter*

The seasonal cycles of primary and secondary production obtained from the three simulations for LSLE, NEG, and MS are shown in Fig. 9. In LSLE, primary production in CDOM simulation is slightly decreased and its peak delayed by one month from REF simulation, accompanied by moderate decrease in secondary production. In CDOM+TEMP simulation, both primary production and secondary production decrease dramatically from REF simulation, with the peak of primary production delayed to July. In NEG, the seasonal cycle of primary and secondary production are quite the same between REF and CDOM simulations. In CDOM+TEMP simulation, the peaks of primary production and secondary production are decreased and delayed comparing with REF and CDOM simulations. In MS, the peaks of primary and secondary production in CDOM+TEMP simulation are delayed, but increased from REF and CDOM simulations.

Fig. 10(a–c) shows the annual mean distributions of primary production of GSL obtained from the three simulations. Annual primary productions are 78.2, 75.1, and 49.6 g C m^{-2}, for REF, CDOM, and CDOM+TEMP simulations, respectively. Annual primary production of CDOM+TEMP simulation is about 67% those of REF and CDOM simulations. In the REF simulation, the highest primary production is in the whole LSLE, including the area west of the CDOM-rich Saguenay River (Fig. 10a). In CDOM simulation, primary production in the LSLE is about 50% of REF simulation, and the area with the highest primary production is limited to the east of Saguenay River (Fig. 10b). Primary productions in the MS are close in REF and CDOM simulations. In CDOM+TEMP simulation, primary production in the LSLE is decreased dramatically, but slightly increased in downstream of the Gaspé current in the southeastern coast of the MS (Fig. 10c). Primary production gradient between LSLE and MS are much smaller in CDOM+TEMP simulation than in REF and CDOM simulations.

The spatial distributions of zooplankton production (Fig. 10d–f) follow those of primary productions (Fig. 10a–c) of the respective simulation. In REF simulation, zooplankton production is concentrated in the LSLE and downstream of Gaspé current (Fig. 10d). In CDOM simulation, the zooplankton production is also concentrated in the LSLE and downstream of Gaspé current, but limited to the area east of Saguenay River (Fig. 10e). Peak zooplankton production of CDOM simulation is about 50% of that in REF simulation in the LSLE. In CDOM+TEMP simulation, high zooplankton production is near the coast of Gaspé peninsula, and downstream of the Gaspé current (Fig. 10f). Zooplankton production in the MS is higher in CDOM+TEMP simulation than in REF and CDOM simulations.

Annual zooplankton productions in the top 50 m of the water column are 19.1, 16.9, and 17.1 g C m^{-2}, for REF, CDOM, and CDOM+TEMP simulations, respectively. In CDOM+TEMP simulation, primary production is about 67% those of REF and CDOM simulations. In contrast, zooplankton production in CDOM+TEMP simulation is quite the same as in REF and CDOM simulations. Therefore, as a result of temperature-regulated plankton growth, more primary production is exported to secondary production in CDOM+TEMP simulation than in REF and CDOM simulations.

The distributions of total sinking flux of organic matter including detrital POM and large phytoplankton, and the percentage of large phytoplankton in the total sinking flux are shown in Fig. 11. The total sinking fluxes are 0.11, 0.16, and 0.09 mmol N m^{-2} d^{-1}, corresponding to 4.0, 6.2, and 5.3% of total primary production, for REF, CDOM, and CDOM+TEMP simulations, respectively. Large phytoplankton account for 56%, 28%, and 26% of the total sinking flux of organic matter, for REF, CDOM, and CDOM+TEMP simulations, respectively (Fig. 11).

4. Discussion

4.1. *Effects of CDOM and temperature on model performance*

The evaluation of model performance is conducted based on two cruises of snapshot field sampling in June and November, the spring and fall bloom seasons of GSL, of 1997. The station by station model-data comparison are semi-quantitative at best, since the hydrodynamics of the water column are highly variable across space scale that may be smaller than model resolution (5 × 5 km). Therefore, we will focus on the effects of CDOM and temperature on the timing of spring phytoplankton bloom and primary and secondary production in the GSL.

The simulated Chl biomass is lower than in observation in LSLE in all three simulations, with the lowest biomass simulated in CDOM+TEMP simulation (Figs. 6 and 7), which caused the high

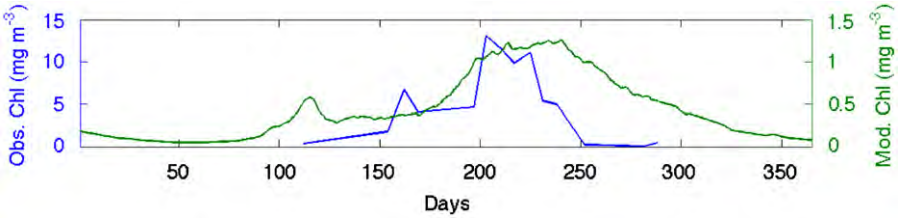

Fig. 7. Time series observation of Chl averaged over the top 50 m of the water column at an estuary station, Rimouski station (blue line, left axis), and mean Chl of upper 50 m of water column of LSLE (green line, right axis) based on CDOM+TEMP simulation throughout 1997. The location of the station is shown as a star in Fig. 1. The observed Chl is redrawn from Starr et al. (2004, Fig. 4). (For interpretation of the references to color in this figure legend, the reader is referred to the web version of this article.)

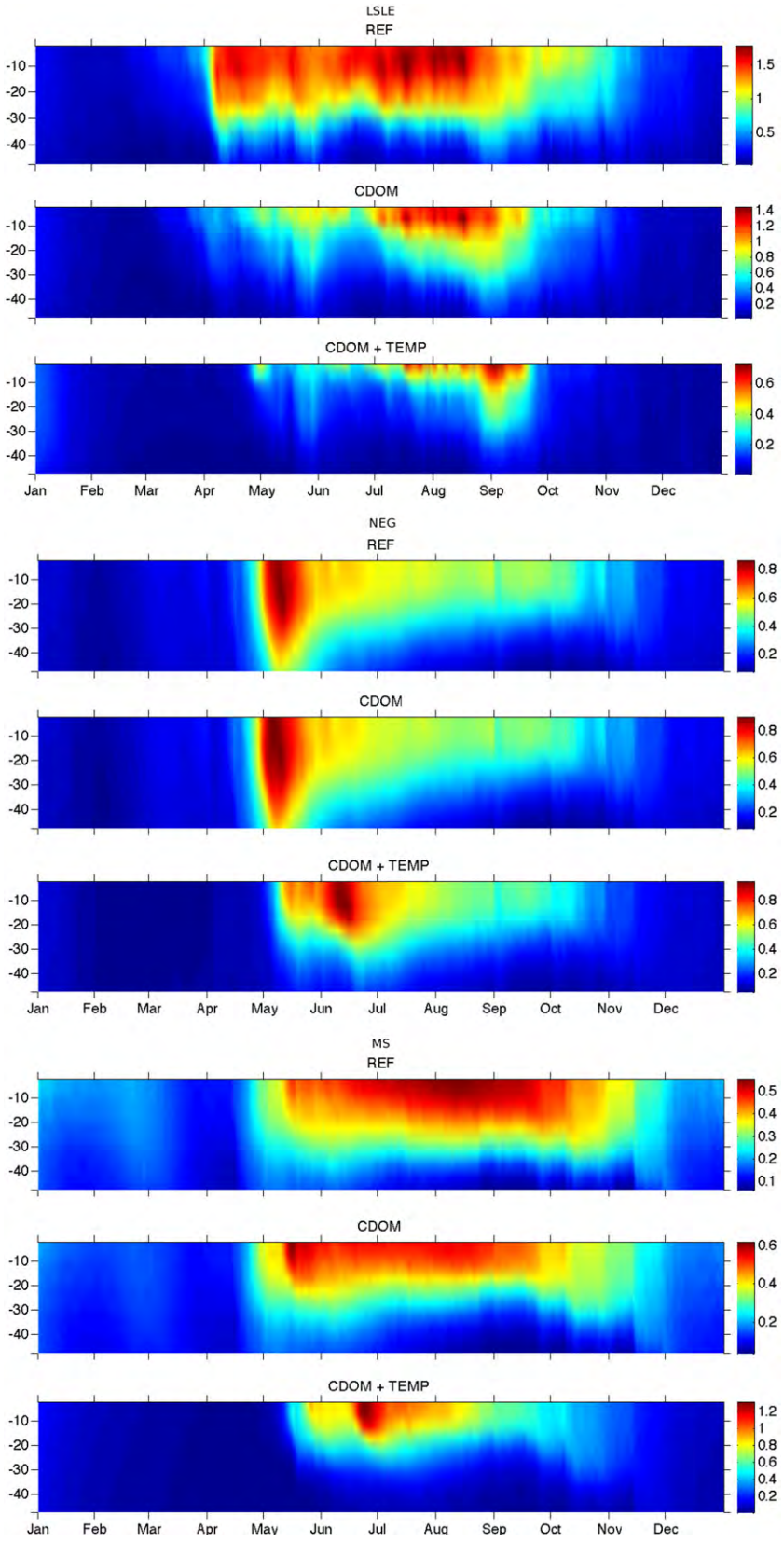

Fig. 8. Time series of zooplankton (micro- plus mesozooplankton) biomass (mmol N m^{-3}) profile integrated over each of the three subregions: LSLE (top), NEG (middle) and MS (bottom) for reference simulation (REF), CDOM simulation (CDOM), and temperature dependent plankton growth simulation (CDOM+TEMP).

RMSD of the three simulations. Based on *RMSD*, it appears that CDOM+TEMP simulation performs worse than CDOM simulation, particularly in spring (Fig. 3). The fact that the standardized bias is lowest in CDOM+TEMP simulation, combined with higher σ, suggests that the higher *RMSD* of CDOM+TEMP simulation than REF and CDOM simulations is caused by overestimating the

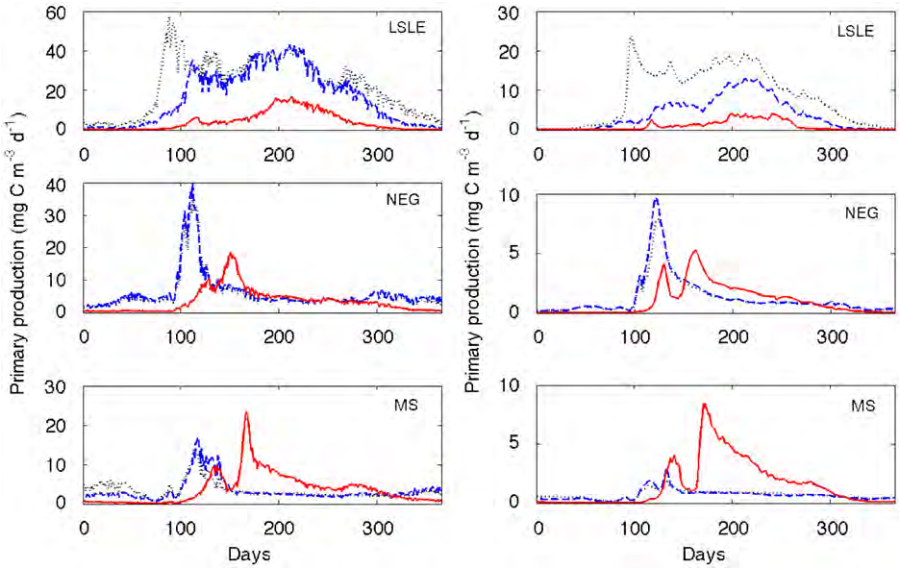

Fig. 9. Seasonal cycles of primary (left) and secondary production (right) in the top 50 m of the water column of LSLE, NEG, and MS. Black dotted line, blue dashed line and red solid line represent REF simulation, CDOM simulation, and CDOM+TEMP simulation, respectively. (For interpretation of the references to color in this figure legend, the reader is referred to the web version of this article.)

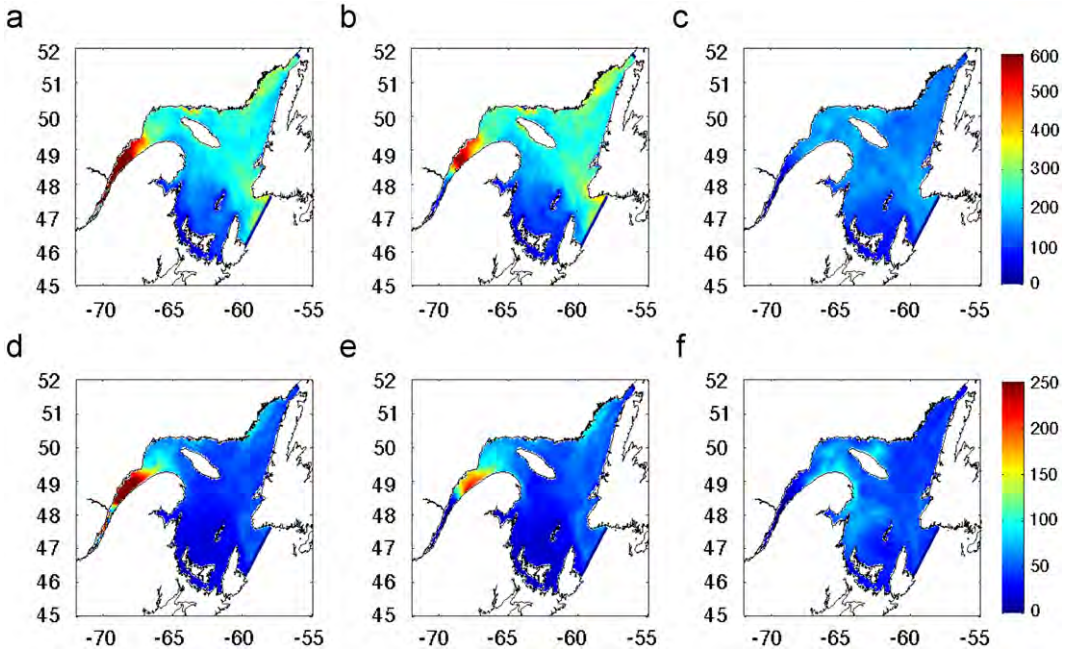

Fig. 10. Spatial distribution of annual mean daily primary production (mg C m^{-2} d^{-1}) for REF (a), CDOM (b), and CDOM+TEMP (c) simulations, and zooplankton production (mg C m^{-2} d^{-1}) for REF (d), CDOM (e), and CDOM+TEMP (f) simulations.

variability in CDOM+TEMP simulation, particularly in June. This is largely due to low Chl simulated in the LSLE in June in CDOM+TEMP simulation. The underestimation of phytoplankton biomass in LSLE during spring bloom will be further discussed below. *R* measures the covariation between model and data. The higher correlation between data and model of CDOM+TEMP simulation than REF and CDOM simulations during spring bloom season suggests that CDOM+TEMP simulation catches the seasonal cycle and spatial variations of phytoplankton biomass in the GSL better than REF and CDOM simulations. Figs. 6 and 7 show that CDOM+TEMP simulation catches the timing of spring phytoplankton bloom better than REF and CDOM simulations.

4.2. What controls the timing of spring phytoplankton bloom?

Regarding the advection hypothesis, the timing of spring phytoplankton bloom is simulated with the same realistic advection generated by the 3-D circulation model of Saucier et al. (2003). The timing of spring phytoplankton bloom simulated with 3-D coupled circulation model should not be explained by advection alone, as the dynamic of phytoplankton biomass is the result of growth, consumption and advection. The results of REF simulation suggest under realistic advection phytoplankton bloom in LSLE should start in March–April (Fig. 6 top), which is much earlier than that observed in June–July (Fig. 7).

In the REF simulation, non-pigment associated detrital light attenuation (k_p) is set as constant (Table 2), which is low compared to light absorption by CDOM. Therefore, in the CDOM simulation, CDOM is assumed to be the prominent non-pigment light attenuation component. Since the contribution of detritus to total light absorption by particulate materials is inversely related to phytoplankton biomass in GSL (Roy et al., 2008), particulate light absorption in the water is dominated by phytoplankton pigments in phytoplankton bloom season. Therefore, ignoring k_p in CDOM and CDOM+TEMP simulations should not affect the timing of phytoplankton bloom significantly. After the spring bloom, particulate detritus may become a significant component of light attenuation in the water column. Phytoplankton growth then, however, is limited by nutrient in stratified water column.

The results of CDOM simulation suggest that if turbidity due to CDOM is taken into account, spring phytoplankton bloom should start in late April–early May (Fig. 6). This is because the mean irradiance in the mixed layer is higher than critical light intensity required for net phytoplankton growth in April and May (Levasseur et al., 1984). Fig. 12 shows that the simulated mean irradiance in the euphotic zone of the LSLE reaches the *ke* (10 Einst m^{-2} d^{-1}, see Table 2) after April in CDOM and CDOM+TEMP simulations. Therefore, CDOM can only partly explain why spring phytoplankton bloom in the LSLE is delayed compared with that in the Gulf. This is understandable, because phytoplankton growth does not increase with light linearly. CDOM may impose light limitation to phytoplankton growth only when PAR is reduced to the linear range of PAR-phytoplankton growth response curve before April.

Temperature regulation of phytoplankton and zooplankton growth rates significantly delays the onset of spring phytoplankton bloom particularly in the LSLE, because the LSLE is colder than the rest of the GSL throughout the year (Figs. 4 and 5), which is attributed to tidal mixing of cool water of the intermediate layer with surface water at the head of Laurentian Trough (Gratton et al., 1988; Saucier et al., 2003). According to the model of temperature-dependent μ_{max} of phytoplankton (Rose and Caron, 2007), the μ_{max} of phytoplankton is predicted to be at 0.97 d^{-1} at temperature of 7.8 °C, which agrees with Tamigneaux et al. (1997), who observed phytoplankton growth rate of 1.09 d^{-1} based on dilution experiment at that temperature in the GSL. Obviously, the temperature-independent μ_{max} of phytoplankton in REF and CDOM simulations (1.39 d^{-1}, equivalent to doubling time of 0.5 d in Table 2) overestimated phytoplankton growth rate at temperature below 13 °C. That results in early phytoplankton bloom, as light is indeed not limiting since April even when light attenuation due to CDOM is taken into account. Similarly, the temperature independent g_{max}^{MIZ} and g_{max}^{MEZ} in REF and CDOM simulations become underestimated relative to the temperature-regulated maximum grazing rate of Rose and Caron (2007) after temperature is above 5–6 °C. Therefore, the seasonal cycle of water temperature changes not only the growth rate of phytoplankton and zooplankton, but also the differences in the growth rates between

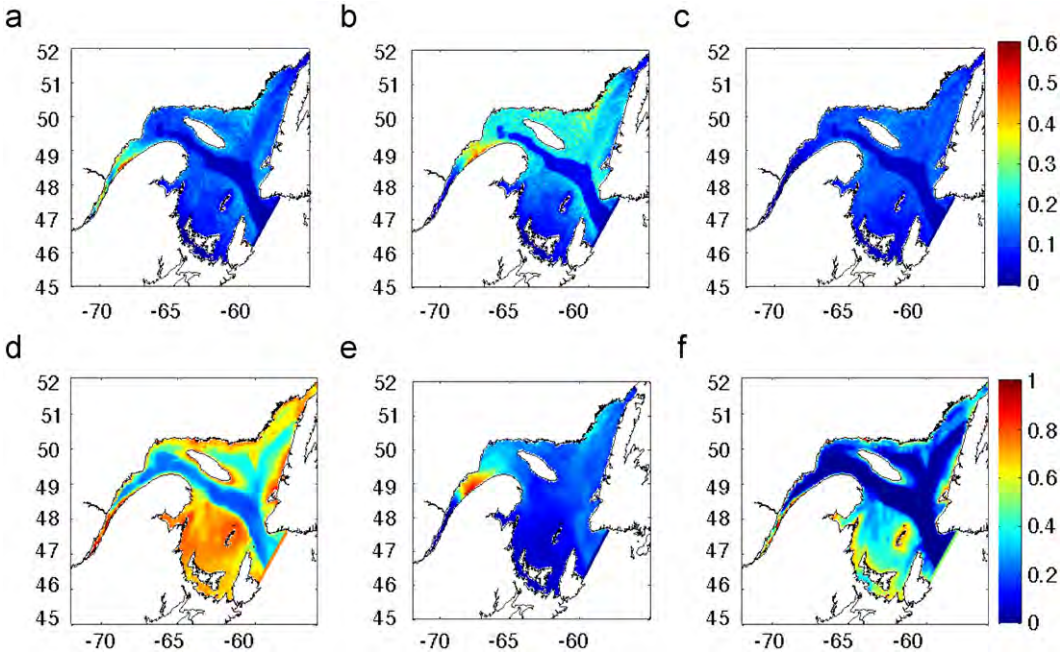

Fig. 11. Spatial distribution of total sinking flux (diatoms+particulate organic nitrogen) (mmol N m^{-2} d^{-1}) for REF (a), CDOM (b), and CDOM+TEMP (c) simulations, and percentage of diatom in total sinking flux, for REF (d), CDOM (e), and CDOM+TEMP simulations (f).

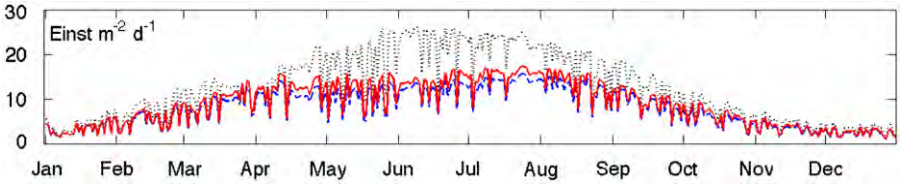

Fig. 12. Time series of simulated mean irradiance in the euphotic zone of LSLE. Black dotted line, blue dashed line and red solid line are for REF simulation, CDOM simulation, CDOM+TEMP simulation, respectively. (For interpretation of the references to color in this figure legend, the reader is referred to the web version of this article.)

phytoplankton and zooplankton, and thus the coupling between autotrophic and heterotrophic productions over the seasonal time scale.

The exact time of the bloom may vary interannually, but there appears to be a consistent regional pattern of the timing of spring phytoplankton blooms in the GSL. That is, it is consistently earlier in the Gulf than in the estuary (Levasseur et al., 1984; Roy et al., 2008). Only CDOM+TEMP simulation can simulate such a regional pattern in the timing of spring phytoplankton bloom. It follows that in addition to advection and CDOM from freshwater discharge, temperature dependent growth of phytoplankton and zooplankton plays an important role in determining the regional differences in the timing of spring phytoplankton bloom in the GSL.

4.3. Biological productivity of the GSL

Primary production obtained in all three simulations are lower than most of the estimates based on field sampling (see Le Fouest et al., 2005, and references therein). Field observations might also have overestimated annual primary production, because sampling are biased toward growth seasons with limited spatial and temporal coverages. Phytoplankton can acclimate to low irradiance by increasing cellular Chl concentration and decreasing the half saturation constant for photosynthesis (Cloern et al., 1995; MacIntyre et al., 2002). Roy et al. (2008) observed differences between light absorption properties of phytoplankton in the LSLE and the Gulf. Acclimation strategies of phytoplankton photosynthesis to reduced irradiance due to CDOM in the water column remained to be further investigated for the GSL. Sensitivity test of the *ke* suggests primary production in the LSLE may increase by 1.8 times due to photoacclimation (Le Fouest et al., 2010). Seasonal cycle of temperature may affect not only growth rate, but also shifts in size–structure, community structure and photosynthetic characteristics (Bouman et al., 2003, 2005; Roy et al., 2008), which should be considered in the future. In the present model, the fixed C:Chl and C:N ratios are assumed. If the C:Chl and C:N vary by a factor of 2, the simulated primary production of organic carbon may vary by a factor of 2 based on the same nutrient supply (Christian, 2005, for example).

CDOM is known to modify the optical properties of the water column and thus primary production in coastal and estuarine waters (Branco and Kremer, 2005; Coble et al., 2003; Tilstone et al., 2005). The effects of CDOM on the biomass and production of primary and secondary producers appear limited to the LSLE, where CDOM reduces phytoplankton production by about 50%. The reduced consumption of NO_3 in the upstream of the Gaspé current (LSLE) leaves unused NO_3 available to phytoplankton in the downstream of Gaspé current along the coast of Gaspé peninsula and MS. That explains why CDOM only slightly reduces overall primary production, but redistributes phytoplankton biomass and production in the GSL. The effects of CDOM on primary production in the rest of the GSL, such as the MS are limited, since phytoplankton further downstream are also nutrient limited. If photobleaching of CDOM (Whitehead et al., 2000) is considered in the model, its effects on primary production would be less.

CDOM and detrital light absorption is high in blue light region, but photosynthetic pigments have a light absorption peak in blue and red light regions. In the future models, the light attenuation due to particulate detritus and CDOM should be better represented. Ideally, a spectrally resolved light absorption and primary production model should be developed to quantify the impact of various optical components in affecting the quantity and quality of light in the water column, and light utilization by phytoplankton (Tilstone et al., 2005, for example).

Lower primary production obtained in CDOM+TEMP simulation may be explained as follows. Firstly, phytoplankton growth is limited by low temperature at the beginning of the growth season. The μ_{max} of phytoplankton based on Rose and Caron (2007) is lower than that in REF and CDOM simulations before temperature is $< 13\ ^{\circ}C$. Secondly, low temperature below the thermocline reduces phytoplankton growth in the lower part of the euphotic zone. Thirdly, the delayed spring phytoplankton bloom due to temperature limitation at low temperature season allows phytoplankton growth to be better matched with zooplankton grazing that increases with temperature. g_{max}^{MES} based on Rose and Caron (2007) is close to that in REF and CDOM simulations when temperature is $< 5\ ^{\circ}C$, and increasingly deviate from REF and CDOM simulations as it increases with temperature as the season progresses. However, zooplankton grazing may not only be constrained by water temperature, but also by hydrodynamics of the water column (Metcalfe et al., 2004). In the GSL estuary, large zooplankton migrate to deep water in order to avoid strong current at surface and to retain in the productive zone (Winkler et al., 2003). Those physical conditions associated with strong current and turbulence may reduce their grazing rate on phytoplankton and growth efficiencies from that set by temperature. That would allow phytoplankton biomass to build up and thus increase primary production in the GSL. More data on the feeding ecology of zooplankton in relation to physical conditions of the water column is needed to parameterize zooplankton grazing rate in the GSL, particularly in the estuary with strong current and turbulent shear.

The lower estimates of primary production in the three simulations are also related to the fact that nutrient input from rivers and freshwater discharge were not considered in the model. The importance of nutrient input from freshwater discharge is debatable, but remains to be resolved. Sinclair et al. (1976) estimated that nutrient input from freshwater discharge accounted for 1–5% of total nutrient required by primary production in the GSL. In the LSLE, 18% of surface NO_3 is estimated to originate from freshwater discharge in summer months (July–September) based on inverse modeling (Savenkoff et al., 2001). The contribution of river nutrient influx to annual primary production of the GSL remains uncertain. However, it has been observed that freshwater discharge has a direct consequence to the biological production of the GSL. For example, the variability of the marine and shellfish landing has been related to freshwater discharge received by the GSL (Drinkwater and Myers, 1987).

The simplified ecosystem model does not have an explicit microbial food-web, and the ultimate food source of zooplankton is phytoplankton only. Particularly in CDOM+TEMP simulation, maximum zooplankton grazing rate increases with temperature over the season. Should the external nutrient input be considered, and microbial food-web be explicitly included in the ecosystem model, zooplankton may obtain part of the food originated from external nutrients via the microbial food-web, and phytoplankton may experience less grazing pressure from zooplankton. That may allow higher phytoplankton biomass in bloom season. Thingstad et al. (2005) reported that inorganic nutrient might bypass phytoplankton and reach mesozooplankton through microbial food-web. It has been reported that during spring phytoplankton bloom, bacterial growth is not limited by substrate, and their grazing mortality were high, suggesting production due to microbial food web contributed significantly to the carbon flux in the GSL (Rivkin et al., 1996). More data is needed to account for the contribution of external nutrient input to the biological production through microbial food web and their impacts on ecosystem structure of GSL.

The match between phytoplankton bloom and increased zooplankton grazing suppresses the phytoplankton biomass, and allows more organic matter produced by large phytoplankton to be transferred to secondary production. That is illustrated in Fig. 11, which shows a reduction in the sinking of large phytoplankton in CDOM+TEMP simulation. Roy et al. (2000) reported during spring phytoplankton bloom, mesozooplankton grazing removes 45% of

primary production in the upper 50 m, indicating a close coupling between primary and secondary production in the GSL. Zooplankton production are 35% of the primary production for CDOM+TEMP simulation, comparing with 24% and 22.5% of the primary production in REF and CDOM simulations, respectively. This indicates that temperature plays an important role in regulating the seasonal development of phytoplankton and zooplankton, and determines the export of primary production to secondary production. Consequently, even though primary production in CDOM+TEMP simulation is 33% lower than in REF and CDOM simulations, the secondary production are close in all the three simulations (Section 3.5).

Our work suggests that the link between freshwater runoff and fisheries production (Bugden et al., 1982; Drinkwater and Myers, 1987) is not limited to nutrient loading only, but also related to CDOM and temperature. The CDOM has complex effects on the biogeochemical cycles of marine ecosystems. CDOM reduces irradiance in the water column, but also mitigates the adverse effects of UV on the phytoplankton photosynthesis and production, transform CDOM into labile dissolved organic matter that is readily available to microbial community (Zepp et al., 2003). There is also evidence that CDOM may be remineralized into CO_2, which causes ocean acidification, rendering phytoplankton more susceptible to photoinhibition, and thus reducing primary production (Sobrino et al., 2009). In the GSL, CDOM redistributes primary production between LSLE and MS with higher primary production in the MS being favored when LSLE receives more CDOM. The interannual variability of seasonal cycles of freshwater runoff and temperature is related to the variation of climate forcing, which has consequence on the seasonal cycles of phytoplankton and zooplankton growth and coupling between phytoplankton and zooplankton production. That will undoubtedly affect the interannual variability of the survival of fish larvae that feed on zooplankton in the GSL.

Similar subarctic inland seas and coastal shelf seas, such as Hudson Bay (Granskog et al., 2007), Irish Sea (Tilstone et al., 2005) and Baltic Sea (Kowalczuk et al., 2006), are affected by biogeochemical processes on the land, and receive large amount of terrestrial organic materials. In the past, most studies focus more on stratification effects and nutrient input due to freshwater runoff than the negative effects of CDOM on the seasonal cycle of phytoplankton biomass and production (Ji et al., 2008, for example). The effects of CDOM on the seasonal cycle of phytoplankton biomass and production may vary depending on specific geographic setting. Therefore, the effects of CDOM on the irradiance of the water column need to be incorporated in the coupled physical-ecosystem model for inland sea ecosystems. Subarctic ecosystems are also characterized with strong seasonal temperature cycles. Most coupled models use Q_{10} of 2 to simulate the temperature effects on the rate of plankton growth. Different slopes for temperature-dependent phytoplankton and zooplankton growth will have consequences to the seasonal cycles of phytoplankton and zooplankton, and the coupling between autotrophic and heterotrophic processes in systems with large seasonal temperature range.

5. Conclusion

The timing and extent of the spring bloom is critical to the overall biological production of marine ecosystems. Model simulations of primary and secondary production in this study of the GSL show that as in other estuarine systems, CDOM from freshwater runoff plays an important role in delaying spring phytoplankton bloom. In the LSLE of the GSL, however, the upwelling of cold water at the head of Laurentian Channel also plays an important role in delaying the spring phytoplankton bloom. The reduced growth of phytoplankton in the LSLE due to a combination of CDOM and low temperature alters the spatial distribution of primary and secondary production in the GSL. Reduced phytoplankton growth, and thus nutrient consumption in the LSLE leaves more nutrient from St. Lawrence river available to downstream of Gapsé current and in the MS. This is consistent with the fact that the MS is a productive fishing ground of GSL which benefits from nutrient input from St. Lawrence river (Levasseur et al., 1992).

CDOM and temperature dependent growth of plankton community are critical in simulating interannual variability of biological productivity in response to interannual variability of climate forcing. Future climate change will change water temperature, precipitation and thus the freshwater runoff to the GSL. When the effects of CDOM and water temperature on the plankton growth are considered in the model, it is able to predict the response of the timing of spring phytoplankton bloom, coupling between the primary production and secondary production, and export of organic matter, to future climate change.

Our model still suffers from underestimation of phytoplankton biomass in LSLE during spring phytoplankton bloom, particularly in CDOM+TEMP simulation. This does not suggest that temperature control of phytoplankton and zooplankton growth is wrong. Instead, it points to other important control mechanisms ignored in the model. In order to fully understand the control mechanisms of the seasonality of phytoplankton and zooplankton production in the GSL, it is necessary to consider the contribution of external nutrients to the GSL through freshwater runoff, and their biogeochemical transformation through microbial food web, and couple the biogeochemical processes into the NPZD model. It is important to understand the control mechanisms of the planktonic ecosystem before tuning model parameters to fit model output to observations.

Acknowledgments

Discussions with Drs. Andrew J. Irwin and Dr. Zoe V. Finkel, and constructive comments and critiques from the three anonymous reviewers are helpful in improving the early versions of the manuscript. The simulations are conducted in ISMER, UQAR, under the project funded by Canadian Space Agency to FJS and BZ. Most of the data analysis and writing are completed while ZPM is working in Marine Macroecology and Biogeochemistry Lab (MMaB) of Mount Allison University. Support from MMab and Mount Allison University are critical for the completion of the work.

References

Blough, N., Del Vecchio, R., 2002. Chromophoric DOM in the coastal environments. In: Hansell, D., Carlson, C. (Eds.), Biogeochemistry of Marine Dissolved Organic Matter. Academic Press, pp. 509–546 (Chapter 10).

Bouman, H., Platt, T., Sathyendranath, S., Li, W., Stuart, V., Fuentes-Yaco, C., Maass, H., Horne, E., Ulloa, O., Lutz, V., Kyewalyanga, M., 2003. Temperature as indicator of optical properties and community structure of marine phytoplankton: implications for remote sensing. Marine Ecology Progress Series 258, 19–30.

Bouman, H., Platt, T., Sathyendranath, S., Stuart, V., 2005. Dependence of light-saturated photosynthesis on temperature and community structure. Deep-Sea Research I 52, 1284–1299.

Branco, A., Kremer, J., 2005. The relative importance of chlorophyll and colored dissolved organic matter (CDOM) to the prediction of the diffuse attenuation coefficient in shallow estuaries. Estuaries 28, 643–652.

Bugden, G., Hargrave, B., Sinclair, M., Tang, C., Therriault, J.-C., Yeats, P., 1982. Freshwater runoff effects in the marine environment: the Gulf of St. Lawrence example. Canadian Technical Report of Fisheries and Aquatic Science, vol. 1078, pp. 1–89.

Caron, D., Rose, J., 2008. The metabolic theory of ecology and algal bloom formation (Reply to comment by Lopóz-Urrutia). Limnology and Oceanography 53, 2048–2049.

Carr, M.-E., Friedrichs, M., Schmeltz, M., Aita, M., Antoine, D., Arrigo, K., Asanuma, I., Aumont, O., Barber, R., Behrenfeld, M., Bidigare, R., Buitenhuis, E., Campbell, J., Ciotti, A., Dierssen, H., Dowell, M., Dunne, J., Esaias, W., Gentili, B., Gregg, W., Groom, S., Hoepffner, N., Ishizaka, J., Kameda, T., LeQuéré, C., Lohrenz, S., Marra, J., Mélin, F., Moore, K., Morel, A., Reddy, T., Ryan, J., Scardi, M., Smyth, T., Turpie, K., Tilstone, G., Watersa, K., Yamanaka, Y., 2006. A comparison of global

estimates of marine primary production from ocean color. Deep-Sea Research II 53, 741–770.
Chadwick, M., Sinclair, A., 1991. Fisheries production in the Gulf of St. Lawrence. In: Therriault, J.-H. (Ed.), The Gulf of St. Lawrence: Small Ocean or Big Estuary? Canadian Special Publication of Fisheries and Aquatic Science, vol. 113, pp. 125–136.
Christian, J.R., 2005. Biogeochemical cycling in the oligotrophic ocean: Redfield and non-Redfield models. Limnology and Oceanography 50, 646–657.
Cloern, J., Grenz, C., Vidergar-Lucas, L., 1995. An empirical model of the phytoplankton chlorophyll: carbon ratio-the conversion factor between productivity and growth rate. Limnology and Oceanography 40, 1313–1321.
Coble, P., Hu, C., Gould, R., Chang, G., Wood, A., 2003. Colored dissolved organic in the coastal ocean. Oceanography 17, 51–59.
Cushing, D., 1990. Plankton production and year-class strength in fish populations—an update of the match mismatch hypothesis. Advances in Marine Biology 26, 249–293.
de Lafontaine, Y., Demers, S., Runge, J., 1991. Pelagic food web interactions and productivity in the Gulf of St. Lawrence: A perspective. Canadian Special Publication of Fisheries and Aquatic Science 113, 99–124.
Dickie, L., Trites, R., 1983. Gulf of St. Lawrence. In: Ecosystems of the World, 26: Estuaries and Semi-enclosed Seas. Elsevier Science Publication, Amsterdam, pp. 403–425.
Doyon, P., Klein, B., Ingram, R.G., Legendre, L., Tremblay, J.-E., Therriault, J.-C., 2000. Influence of wind mixing and upper-layer stratification on phytoplankton biomass in the Gulf of St. Lawrence. Deep-Sea Research II 47, 415–433.
Drinkwater, K., Myers, R., 1987. Testing predictions of marine fish and shellfish landing from environmental variables. Canadian Journal of Fisheries and Aquatic Science 44, 1568–1573.
Eppley, R., 1972. Temperature and phytoplankton growth in the sea. Fishery Bulletin 70, 1063–1085.
Fasham, M., Ducklow, H., McKenzie, S., 1990. A nitrogen-based model of plankton dynamics in the oceanic mixed layer. Journal of Marine Research 48, 591–639.
Friedrichs, M., Carr, M.-E., Barber, R., Scardi, M., Antoine, D., Armstrong, R., Asanuma, I., Behrenfeld, M., Buitenhuis, E., Chai, F., Christian, J., Ciotti, A., Doney, S., Dowell, M., Dunne, J., Gentili, B., Gregg, W., Hoepffner, N., Ishizaka, J., Kameda, T., Lima, I., Marra, J., Melin, F., Moore, K., Moréle, A., O'Malley, R.T., O'Reilly, J., Saba, V., Smyth, T.J., Schmeltz, M., Tjiputra, J., Waters, K., Westberry, T., Winguth, A., 2009. Assessing the uncertainties of model estimates of primary productivity in the tropical pacific ocean. Journal of Marine Systems 76, 113–133.
Frost, B., 1972. Effects of size and concentration of food particles on the feeding behaviour of the marine planktonic copedpod *Calanus pacificus*. Limnology and Oceanography 17, 805–815.
Granskog, M., Macdonald, R., Mundy, C.-J., Barber, D., 2007. Distribution characteristics and potential impacts of chromophoric dissolved organic matter (CDOM) in Hudson Strait and Hudson Bay, Canada. Continental Shelf Research 27, 2032–2050.
Gratton, Y., Mertz, G., Gagné, J., 1988. Satellite observations of tidal upwelling and mixing in the St. Lawrence estuary. Journal of Geophysical Research 93, 6947–6954.
Hansen, P., Bjørnsen, Hansen, B., 1997. Zooplankton grazing and growth: Scaling within the 2−2000 μm body size range. Limnology and Oceanography 42, 687–704.
Houghton, R., Fairbanks, R., 2001. Water sources for Georges Bank. Deep-Sea Research II 48, 95–114.
Ji, R., Davis, C., Chen, C., Townsend, D., Mountain, D., Beardsley, R., 2008. Modeling the influence of low-salinity water inflow on winter–spring phytoplankton dynamics in the Nova Scotian Shelf—Gulf of Maine region. Journal of Plankton Research 30, 1399–1416.
Kieber, R., Hydro, L., Seaton, P., 1997. Photooxidation of triglycerides and fatty acids in seawater: implication toward the formation of marine humic substances. Limnology and Oceanography 42, 1454–1462.
Kiefer, D., Mitchell, B., 1983. A simple steady-state description of phytoplankton growth based on absorption cross section and quantum efficiency. Limnology and Oceanography 28, 770–776.
Kiorbøe, T., Mohlenberg, F., Hamburger, K., 1985. Bioenergetics of the planktonic copepod *Acartia tonsa*: relationship between feeding, egg production and respiration, and composition of specific dynamic action. Marine Ecology Progress Series 26, 85–97.
Koutitonsky, V., Bugden, G., 1991. The physical oceanography of the Gulf of St. Lawrence: a review with emphasis on the synoptic variability of the motion, vol. 113. Canadian Special Publication of Fisheries and Aquatic Sciences, pp. 57–90.
Kowalczuk, P., Stedmon, C., Markager, S., 2006. Modeling absorption by CDOM in the Baltic Sea from season, salinity and chlorophyll. Marine Chemistry 101, 1–11.
Le Fouest, V., Zakardjian, B., Saucier, F., 2005. Seasonal vs synoptic variability in plankton production in a high-latitude marginal sea: the Gulf of St. Lawrence (Canada). Journal of Geophysical Research 110, C09012 DOI:10.1029/2004JC002423.
Le Fouest, V., Zakardjian, B., Saucier, F., 2010. Plankton ecosystem response to freshwater-associated bulk turbidity in the subarctic Gulf of St. Lawrence (Canada): a modelling study. Journal of Marine Systems 81, 75–85.
Le Fouest, V., Zakardjian, B., Saucier, F., Çizmeli, S., 2006. Application of SeaWiFS- and AVHRR-derived data for mesoscale and regional validation of a 3-d high-resolution physical–biological model of the Gulf of St. Lawrence (Canada). Journal of Marine Systems 60, 30–50.
Lehrter, J., Pennock, J., McManus, G., 1999. Microzooplankton grazing and nitrogen excretion across a surface estuarine–coastal interface. Estuaries 22, 113–125.
Levasseur, M., Fortier, L., Therriault, J.-C., Harrison, P., 1992. Phytoplantkon dynamics in a coastal jet frontal region. Marine Ecology Progress Series 86, 283–295.
Levasseur, M., Therriault, J.-C., Legendre, L., 1984. Hierarchical control of phytoplankton succession by physical factors. Marine Ecology Progress Series 19, 211–222.
López-Urrutia, A., 2008. The metabolic theory of ecology and algal bloom formation. Limnology and Oceanography 53, 2046–2047.
MacIntyre, H., Kana, T., Anning, T., Geider, R., 2002. Photoacclimation of photosynthesis irradiance response curves and photosynthetic pigments in microalgae and cyanobacteria. Journal of Phycology 38, 17–38.
Metcalfe, A., Pedley, T., Thingstad, T., 2004. Incorporating turbulence into a plankton foodweb model. Journal of Marine Systems 49, 105–122.
Mitchell, M., Harrison, G., Pauley, K., Gagné, P., Maillet, G., Strain, P., 2002. Atlantic zone monitoring program sampling protocol. Technical Report, Bedford Institute of Oceanography.
Morel, A., 1988. Optical modeling of the upper ocean in relation to its biogenous matter content (Case I water). Journal of Geophysical Research 93, 10749–10768.
Nelson, N., Siegel, D., 2002. Chromophoric DOM in the open ocean. In: Hansell, D., Carlson, C. (Eds.), Biogeochemistry of Marine Dissolved Organic Matter. Academic Press, pp. 509–546 (Chapter 8).
Nieke, B., Reuter, R., Heuermann, R., Wang, H., Babin, M., Therriault, J., 1997. Light absorption and fluorescence properties of chromophoric dissolved organic matter (CDOM) in the St. Lawrence estuary (Case 2 waters). Continental Shelf Research 17, 235–252.
Parsons, T.R., Takahashi, M., Hargrave, B., 1984. Biological Oceanographic Processes. Elsevier, New York.
Petrie, B., Yeats, P., 2000. Annual and interannual variability of nutrients and their estimated fluxes in the Scotian Shelf—Gulf of Maine region. Canadian Journal of Fisheries and Aquatic Sciences 57, 2536–2546.
Pickard, T., Chen, W., Blasco, D., Sevenkoff, C., Vézina, A., Tian, R., St-Amand, L., Roy, S., Lovejoy, C., Klein, J.-C., Legendre, L., Ingram, R., 2000. Dissolved organic carbon in the Gulf of St. Lawrence. Deep-Sea Research II 47, 435–459.
Platt, T., Fuentes-Yaco, C., Frank, K., 2003. Spring algal bloom and laval fish survival. Nature, 398–399.
Riegman, R., Kuipers, B., Nooedeloos, A., Witte, H., 1993. Size-differential control of phytoplankton and the structure of plankton communities. Netherland Journal of Sea Research 31, 255–265.
Rivkin, R., Legendre, L., Deibel, D., Tremblay, J., Klein, B., Crocker, K., Roy, S., Silverberg, N., Lovejoy, C., Mesple, F., Romero, N., Anderson, M., Matthews, P., Vezina, A., S, C., Therriault, J., Wesson, J., Berube, C., Ingram, R., 1996. Vertical flux of biogenic carbon in the ocean: is there food web control? Science 272 1163–1166.
Rose, J., Caron, D., 2007. Does low temperature constrain the growth rates of heterotrophic protists? Evidence and implications for algal blooms in cold waters. Limnology and Oceanography 52, 886–895.
Roy, S., Blouin, F., Jacques, A., Therriault, J., 2008. Absorption properties of phytoplankton in the Lower Estuary and Gulf of St. Lawrence (Canada). Canadian Journal of Fisheries and Aquatic Sciences 65, 1721–1737.
Roy, S., Silverberg, N., Romero, N., Deibel, D., Klein, B., Savenkoff, C., Vézina, A., Tremblay, J.-E., Legendre, L., Rivkin, R., 2000. Importance of mesozooplankton feeding for the downward flux of biogenic carbon in the Gulf of St. Lawrence (Canada). Deep-Sea Research II 47, 519–544.
Saíz, E., Alcaraz, M., 1992. Enhanced excretion rates induced by small-scale turbulence in *Acartia* (Copepoda: Calanoida). Journal of Plankton Research 14, 681–689.
Saucier, F., Roy, F., Gilbert, D., Pellerin, P., Ritchie, H., 2003. Modeling the formation and circulation processes of water masses and sea ice in the Gulf of St. Lawrence, Canada. Journal of Geophysical Research 108, 3269 . doi:10.1029/2000JC000686.
Savenkoff, C., Vézina, A., Gratton, Y., 1997. Effect of a freshwater pulse on mesoscale circulation and phytoplankton distribution in the lower St. Lawrence Estuary. Journal of Marine Research 55, 353–381.
Savenkoff, C., Vézina, A., Smith, P., Han, G., 2001. Summer transports of nutrients in the Gulf of St. Lawrence estimated by inverse modeling. Estuarine, Coastal and Shelf Science 52, 53–587.
Sinclair, M., El-Sabh, M., Brindle, J.-R., 1976. Seaward nutrient transport in the lower St. Lawrence Estuary. Journal of Fisheries Research Board of Canada 33, 1271–1277.
Smayda, T., 1970. The suspension and sinking of phytoplankton in the sea. Marine Biology, Annual Review 8, 353–414.
Smyth, T., Tilstone, G., Groom, S., 2005. Integration of radiative transfer into satellite models of ocean primary production. Journal of Geophysical Research—Ocean 110, C10014 . doi:10.1029/2004JC002784.
Sobrino, C., Neale, P.J., Phillips-Kress, J., Moeller, R., Porter, J., 2009. Elevated CO_2 increases sensitivity to ultraviolet radiation in lacustrine phytoplankton assemblages. Limnology and Oceanography 54, 2448–2459.
Starr, M., St-Amand, L., Devine, L., Bérard-Therriault, L., Galbraith, P., 2004. State of phytoplankton in the Estuary and Gulf of St. Lawrence during 2003. Technical Report, Institut Maurice-Lamontagne, Department of Fisheries and Ocean Canada.
Steven, D., 1971. International biological program study of the Gulf of St. Lawrence. In: Hassan, E. (Ed.), Second Gulf of St. Lawrence Workshop. Bedford Institute of Oceanography, Dartmouth, N.S.
Strom, S., Brainard, M., Holmes, J., Olson, M., 2001. Phytoplankton blooms are strongly impacted by microzooplankton grazing in coastal North Pacific waters. Marine Biology 138, 355–368.
Tamigneaux, E., Mingelbier, M., Klein, B., Legendre, L., 1997. Grazing by protists and seasonal changes in the size structure of protozooplankton and phytoplankton

in a temperate nearshore environment (western Gulf of St. Lawrence, Canada). Marine Ecology Progress Series 146, 231–247.
Taylor, K., 2001. Summarizing multiple aspects of model performance in a single diagram. Journal of Geophysical Research—Atmospheres 106D, 7183–7192.
Therriault, J., Levasseur, M., 1985. Control of phytoplankton production in the lower St. Lawrence estuary: light and freshwater runoff. Le Naturaliste Canadien 112, 65–76.
Thingstad, T.F., Krom, M., Mantoura, R., Flaten, G., Groom, S., Herut, B., Kress, N., Law, C., Pasternak, A., Pitta, P., Psarra, S., Rassoulzadegan, F., Tanaka, T., Tselepides, A., Wassmann, P., Woodward, E., Wexels Riser, C., Zodiatis, G., Zohary, T., 2005. Nature of phosphorus limitation in the ultraoligotrophic eastern mediterranean. Science 309, 1068–1071.
Tian, R., 2006. Toward standard parameterizations in marine biological modeling. Ecological Modelling 193, 363–386.
Tilstone, G., Smyth, T., Gowen, R., Martinez-Vicente, V., Groom, S., 2005. Inherent optical properties of the irish sea and their effect on satellite primary production algorithms. Journal of Plankton Research 27, 1127–1148.
Tremblay, L., Gagné, J., 2009. Organic matter distribution and reactivity in the waters of a large estuarine system. Marine Chemistry 116, 1–12.
Turner, J., 2002. Zooplankton fecal pellets, marine snow and sinking phytoplankton blooms. Aquatic Microbial Ecology 27, 57–102.
Whitehead, R., de Mora, S., Demers, S., Gosselin, M., Monfort, P., Mostajir, B., 2000. Interactions of ultraviolet-B radiation, mixing, and biological activity on photobleaching of natural chromophoric dissolved organic matter: a mesocosm study. Limnology and Oceanography 45, 278–291.
Winkler, G., Dodson, J., Bertrand, N., Thivierge, D., Vincent, W., 2003. Trophic coupling across the St. Lawrence River estuarine transition zone. Marine Ecology Progress Series 251, 59–73.
Yeats, P., 1988. Distribution and transport of suspended particulate matter. In: Chemical Oceanography of the Gulf of St. Lawrence, Chemical Oceanography of the Gulf of St. Lawrence, vol. 220, pp. 15–28.
Zakardjian, B., Gratton, Y., Vézina, A., 2000. Late spring phytoplankton bloom in the Lower St. Lawrence Estuary: the flushing hypothesis revisited. Marine Ecology Progress Series 192, 31–48.
Zepp, R., Callaghan, T., Erickson III, D., 2003. Interactive effects of ozone depletion and climate change on biogeochemical cycles. Photochemistry and Photobiological Science 2, 51–61.